Synthesis and formation mechanism of Zn_2SiO_4 nanorods

Shaoyan Zhang[1], Haiyan Kang[2], Yanlei Gao[1]

[1]*College of Chemical Engineering, Shijiazhuang University, Shijiazhuang, Hebei 050035, People's Republic of China*
[2]*School of Municipal and Environment Engineering, Henan University of Urban Construction, Pingdingshan, Henan 467036, People's Republic of China*
E-mail: zsyedu@hotmail.com

Published in Micro & Nano Letters; Received on 21st May 2014; Revised on 18th September 2014; Accepted on 6th October 2014

Zinc silicate (Zn_2SiO_4) nanorods with diameters of 90–100 nm and lengths of up to 600–700 nm have been successfully prepared by a simple hydrothermal route without the assistance of any templates or surfactants. The characterisations of the products were carried out by X-ray diffraction (XRD), field-emission scanning electron microscopy and transmission electron microscopy technology. On the basis of XRD and scanning electron microscopy analyses of the products at different reaction time periods, an Ostwald ripening mechanism is proposed to elucidate the formation mechanism of the nanorod structure. The electrochemical performance of the as-prepared Zn_2SiO_4 nanorods was investigated by a galvanostatic charge–discharge method. The results have shown that the Zn_2SiO_4 nanorods exhibited a higher discharge capacity and better cyclability than the Zn_2SiO_4 bulk materials.

1. Introduction: In the past few decades, zinc silicate (Zn_2SiO_4) has attracted a great deal of attention because of its unique chemical and physical properties, being environmentally benign and low cost, and has been widely applied in various fields, such as the important crystalline phase in glass ceramics [1], paints [2], adsorbents [3], rubber mixtures [4], lithium-ion batteries (LIBs) [5] and luminescent phosphors [6–10]. Traditionally, Zn_2SiO_4 or Zn_2SiO_4-based phosphors were prepared by a high-temperature solid-state reaction by sintering a mixture of appropriate oxides with silica at temperatures above 1000°C for tens of hours [11, 12]. However, this method requires a high reaction temperature, the morphologies of the products are usually irregular microstructures, and the particle size distribution is uneven.

In recent years, the preparation of one-dimensional (1D) nanostructured Zn_2SiO_4-based materials has attracted global interest because of their special physicochemical properties and potential applications in nanodevices. Among the various techniques for preparing 1D nanostructures, hydrothermal synthesis has been proven to be an efficient strategy in terms of low cost, controllable morphology, narrow grain size distribution, high purity and high crystallinity [13, 14]. For example, Qian's and Wang's groups hydrothermally synthesised 1D Zn_2SiO_4 using sodium dodecyl sulphate and cetyltrimethylammonium bromide, respectively, as structure-directing agents [15, 16]. Xu *et al.* [17] reported the synthesis of Zn_2SiO_4 rods by the hydrothermal process using the mixed solvent of ethidene diamine and H_2O. An *et al.* prepared Mn-doped Zn_2SiO_4 nanowires through a hydrothermal route followed by a 'heat treatment process' [18]. These Zn_2SiO_4 products were exclusively achieved by the hydrothermal process with the assistance of an organic template, or with subsequent 'heat treatment', which made the scale-up synthesis more difficult. Therefore, developing a facile, economic and effective strategy to synthesise Zn_2SiO_4 1D nanostructures is of great importance.

In this Letter, we report on a simple template-free hydrothermal method for the large-scale synthesis of Zn_2SiO_4 nanorods. The as-prepared Zn_2SiO_4 nanorods have an average diameter of about 100 nm, and the length of the nanorods is about 600 nm. An 'Ostwald ripening' growth mechanism has been proposed to explain the formation process of Zn_2SiO_4 nanorods based on the composition and shape evolution. Furthermore, the electrochemical properties of this material as an anode material have been investigated in lithium-ion batteries (LIBs). The results have shown that the Zn_2SiO_4 nanorods exhibited a higher discharge capacity and better cyclability than the Zn_2SiO_4 bulk materials, indicating that they are promising anode candidates for LIBs.

2. Experimental: All chemicals were of analytical grade and used as purchased without further purification. Amorphous silica nanoparticles were 'prepared' via the conventional 'Stöber' method [19]. To prepare Zn_2SiO_4 nanorods, 2 mmol silica nanoparticles was added into 10 ml of 0.4 M aqueous solution; the pH value of this suspension was about 4. Then, the pH of the suspension was adjusted to about 10 using a NaOH solution (2 M). After 10 min of stirring, the precursor suspension was transferred into a 25 ml Teflon-lined autoclave, sealed and maintained at 220°C for 24 h. After the reaction, the autoclave was cooled down naturally to room temperature. The obtained products were separated by centrifugation and rinsed several times using deionised water and ethanol, and then vacuum dried at 60°C for 4 h. For comparison, a bulk Zn_2SiO_4 sample was synthesised by a traditional solid-state reaction method by mixing ZnO and SiO_2 in a molar ratio of 2:1, followed by heat treatment at 1300°C for 8 h in an air atmosphere.

The crystal structures of the final products were investigated by X-ray diffraction (XRD, Bruker D8 Advance). The morphologies and sizes of the final products were determined by field-emission scanning electron microscopy (FESEM, Hitachi S-4800) and transmission electron microscopy (TEM, JEOL 2100F).

Electrochemical tests were conducted with coin cells (type 2032). The working electrode was fabricated by compressing a mixture of the active materials, conductive material [acetylene black (ATB)] and binder [polytetrafluoroethylene (PTFE)] in a weight ratio of active material:ATB:PTFE = 8:1:1. The electrolyte was 1 M $LiPF_6$ in a 1:1 mixture of ethylene carbonate (EC)–dimethyl carbonate (DMC); the separator was Celgard 2400. The cells were cycled on a Land battery test system (CT2001A) between 0.02 and 2.5 V against Li^+/Li.

3. Results and discussion: Fig. 1*a* shows the typical XRD pattern of the as-prepared Zn_2SiO_4 nanorods. All peaks in this pattern can be assigned to the pure phase of Zn_2SiO_4 with the rhombohedral structure (JCPDS No. 37–1485). The major XRD diffraction peaks at $2\theta = 25.71°$, 31.72°, 34.09° and 39.01° corresponding to the (220), (113), (410) and (223) planes, respectively, can be seen clearly. No impurity peaks from other phases were detected, indicating the high purity of the product and completed reaction

doi: 10.1049/mnl.2014.0250

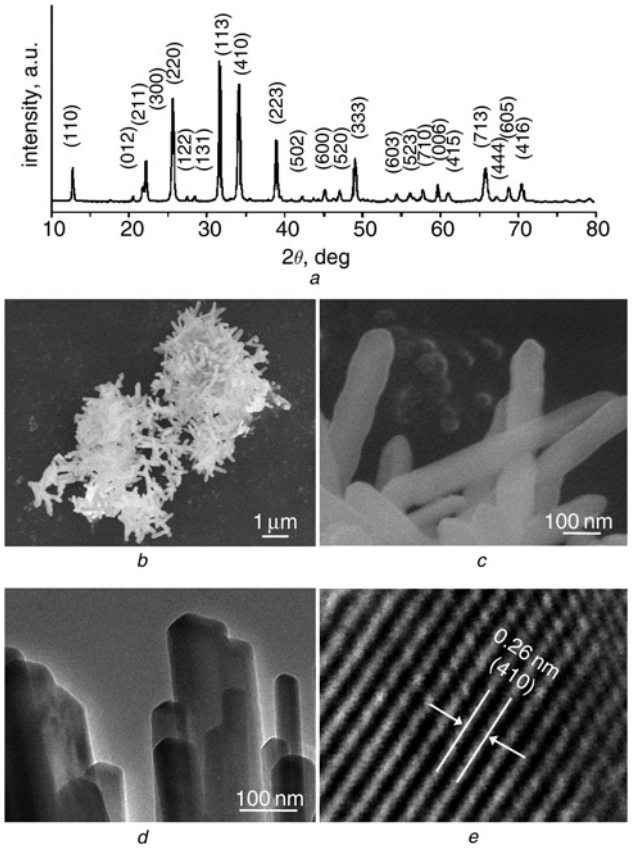

Figure 1 *XRD, FESEM, TEM and HRTEM images of the as-prepared Zn_2SiO_4 nanorods*
a XRD pattern
b and *c* Low and high magnification FESEM images
d and *e* TEM and HRTEM images

during the process. The morphologies of the products were characterised using FESEM and TEM, the corresponding images are shown in Figs. 1*b*–*e*. Fig. 1*b* shows a panoramic FESEM image of the Zn_2SiO_4 nanorods, which is composed of uniform nanorods with lengths in the range of 600–700 nm. A higher magnification image (Fig. 1*c*) shows that the diameter of the rods is in the range of 90–100 nm. Fig. 1*d* displays a representative

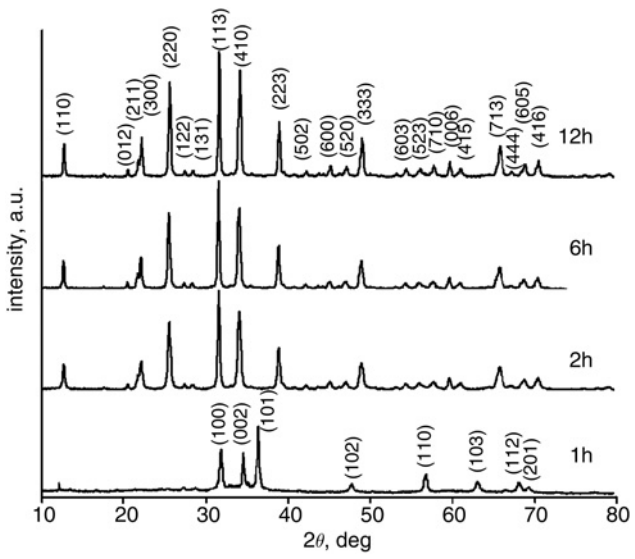

Figure 2 *XRD patterns of the products obtained at different reaction times*

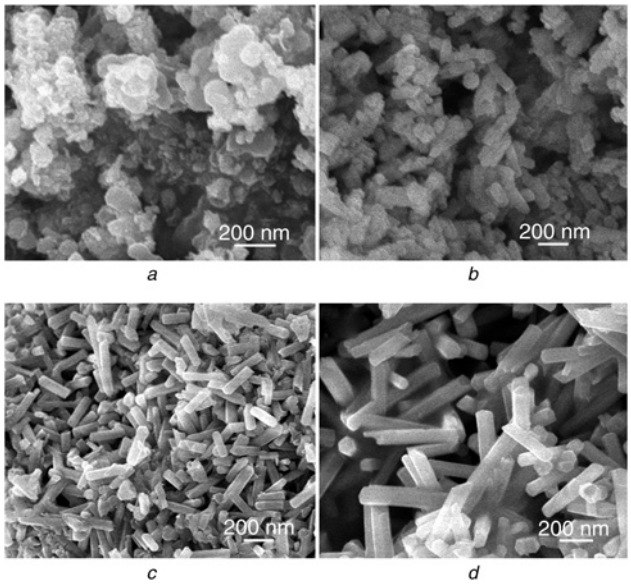

Figure 3 *FESEM images of the products obtained at different reaction times*
a-d 1, 2, 6 and 12 h

TEM image of the as-prepared Zn_2SiO_4 nanorods. It can be seen that the surface of the Zn_2SiO_4 nanorods is smooth. The clearly resolved lattice fringe in Fig. 1*e* was calculated to be about 0.26 nm, corresponding to the (410) plane of rhombohedral structured Zn_2SiO_4.

To study the growth mechanism of Zn_2SiO_4 nanorods, time-dependent experiments were carried out. Figs. 2 and 3 show the XRD patterns and FESEM images of the products hydrothermally synthesised at 220°C for 1, 2, 6 and 12 h. As shown in Fig. 2, at the initial 1 h, all the diffraction peaks in the experimental pattern can be assigned to the pure hexagonal phase of ZnO (JCPDS No. 36-1451). No SiO_2 diffraction peaks were observed, indicating the SiO_2 is still amorphous. Fig. 3*a* shows the FESEM image of the product synthesised at 220°C for 1 h. It is noted that the product is composed of small irregular-shaped nanoparticles and sphere-like particles. It is speculated that the irregular-shaped nanoparticles are ZnO and the sphere-like particles are SiO_2. After 2 h of hydrothermal reaction, the diffraction peaks for ZnO completely vanished, all diffraction peaks can be assigned as pure rhombohedral Zn_2SiO_4, indicating the formation of Zn_2SiO_4. The FESEM image (Fig. 3*b*) shows that the product consists of the nanoparticles and short nanorods. The average diameter of the short nanorods is about 100 nm, and the length is about 200 nm. With the reaction time extended to 6 h, the Zn_2SiO_4 'peaks' became sharper, suggesting an increase in crystallinity. The FESEM shows that most of the nanoparticles disappeared and the length of the nanorods increased to about 300 nm (Fig. 3*c*). By prolonging the reaction time to 12 h, the Zn_2SiO_4 nanorods grew up to about 400 nm (Fig. 3*d*). The results indicate that the crystallinity and the length of the Zn_2SiO_4 nanorods increase with further increased reaction time, and Zn_2SiO_4 nanorods with good crystallinity and lengths of up to about 600 nm were obtained after 24 h of hydrothermal reaction (Fig. 1*b*).

On the basis of the above experimental results, the formation mechanism of the Zn_2SiO_4 nanorods can be proposed. Fig. 4 schematically illustrates the formation process of the Zn_2SiO_4 nanorods. Initially, $Zn(OH)_2$ is formed by the rapid precipitation of the Zn^{2+} and OH^- sources at room temperature. Next, $Zn(OH)_2$ decomposes into ZnO under high-temperature and high-pressure 'hydrothermal' conditions. Then, Zn_2SiO_4 nuclei are formed with the reaction of ZnO and amorphous SiO_2, and then grow into nanoparticles. The

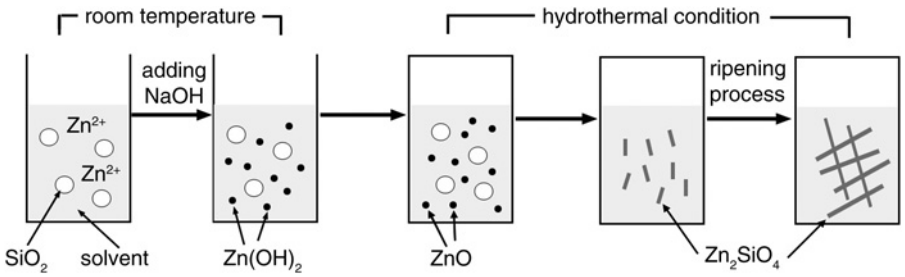

Figure 4 *Schematic illustration of the formation mechanism of Zn_2SiO_4 nanorods*

anisotropic growth habit of Zn_2SiO_4 leads to the oriented aggregation, and these Zn_2SiO_4 nanoparticles developed into rod-like nanostructures under hydrothermal conditions. The growth mechanism of Zn_2SiO_4 nanorods is the well-known 'Ostwald-ripening process', in which the nanorods grew at the cost of the small particles, because of the energy difference in solubility between the large particles and the smaller particles, according to the well-known Gibbs-Thomson law [20, 21].

It was found that the pH values in the solution can influence the morphologies of the products. Fig. 5 shows the morphologies and XRD patterns of the products obtained at different pH values. When the pH value of the precursor suspension was adjusted to 5, the product consisted of well-dispersed nanoparticles with size of ~100 nm (Fig. 5*a*). When adjusting the pH to 14, urchin-like microspheres with an average diameter of 6–8 μm were obtained (Fig. 5*b*). XRD patterns of the products obtained at pH 5 and 14 could be identified as the pure rhombohedral structure of Zn_2SiO_4 (Fig. 5*c*).

The influence of the reaction temperature on the phase composition of the products has also been investigated. Figs. 6 and 7 show the XRD patterns and FESEM images of the products prepared at different temperatures for 24 h, respectively. At a lower reaction temperature of 140°C, the phase of $Zn_4Si_2O_7(OH)_2{\cdot}H_2O$ was mainly synthesised, and small amounts of Zn_2SiO_4 appeared as the secondary phase. The morphology of the product was shown to be a coexistence of microrods and lots of rod-like nanoparticles (Fig. 7*a*). These nanoparticles are about 100 nm in 'diameter' and 200 nm in 'length'. The microrod has a diameter of about 1 μm and a length of several micrometres. With increasing the reaction temperature to 160°C (Fig. 7*b*), the diffraction peaks for $Zn_4Si_2O_7(OH)_2{\cdot}H_2O$ completely vanished, the diffractions peaks can be readily assigned to rhombohedral Zn_2SiO_4. All samples exhibit a rod-like shape, with diameters of 90–100 nm and lengths of 200–300 nm. The result indicates that pure rhombohedral-structured Zn_2SiO_4 can be synthesised even at low a temperature of 160°C, which is much lower than that for the conventional solid-state reaction method. With the reaction temperature increased from 160 to 180°C, the intensity of the diffraction peaks gradually increased and the length of the nanorods increased to about 300 nm (Fig. 7*c*). The result indicates that both the crystallinity and the length of the Zn_2SiO_4 nanorods increase with increasing reaction temperature. Zn_2SiO_4 nanorods with good crystallinity and lengths up to about 400 nm were obtained with increasing reaction temperature to 200°C (Fig. 7*d*). On the basis of the above discussion we can 'speculate' that $Zn_4Si_2O_7(OH)_2{\cdot}H_2O$ forms more readily at relatively low temperatures, 'similar results' have also 'been reported' by Yoon and Kang [6]. In contrast, at a higher temperature of 220°C, $Zn_4Si_2O_7(OH)_2{\cdot}H_2O$ is not detected at different reaction times, which means that the higher temperature favours the formation of Zn_2SiO_4.

To investigate the application of the as-prepared Zn_2SiO_4 nanorods in LIBs, the products were configured as an anode to evaluate their electrochemical properties. Fig. 8*a* displays the charge–discharge curves of the Zn_2SiO_4 nanorods in the first two cycles in the voltage range of 0.02–2.5 V at a current density of 80 mA g^{-1}. As shown in Fig. 8*a*, there was a wide, steady discharging plateau at about 0.6 V (against Li^+/Li) in the first cycle, followed by a gradual voltage decrease. The discharge and charge capacities of

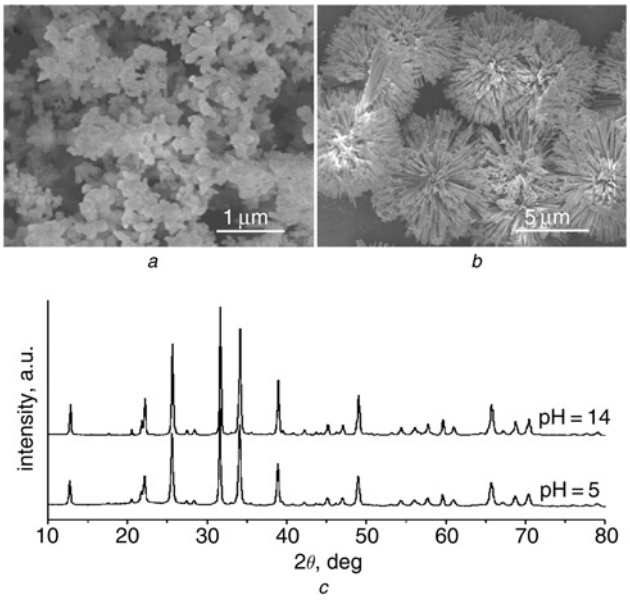

Figure 5 *FESEM images and XRD patterns of the products obtained at different pH values*
a FESEM image at pH 5
b FESEM image at pH 14
c XRD patterns

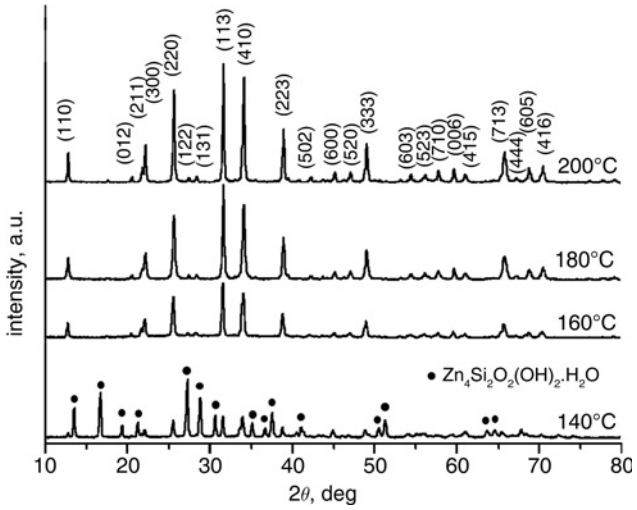

Figure 6 *XRD patterns of the products obtained at different temperatures*

doi: 10.1049/mnl.2014.0250

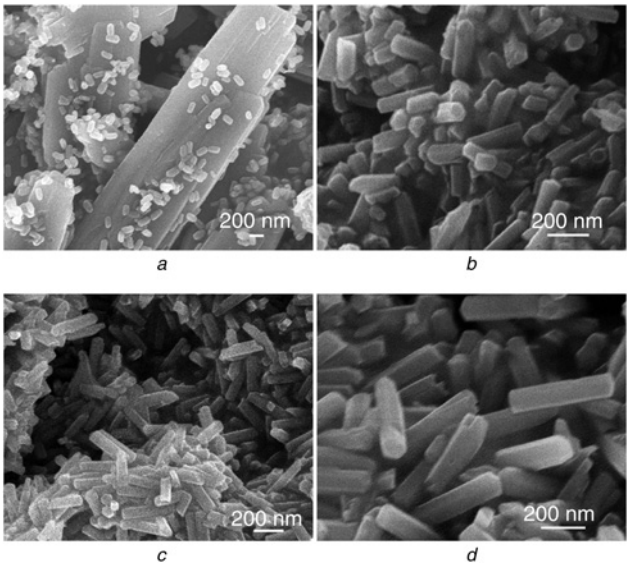

Figure 7 *FESEM images of the products obtained at different temperatures a-d* 140, 160, 180 and 200°C

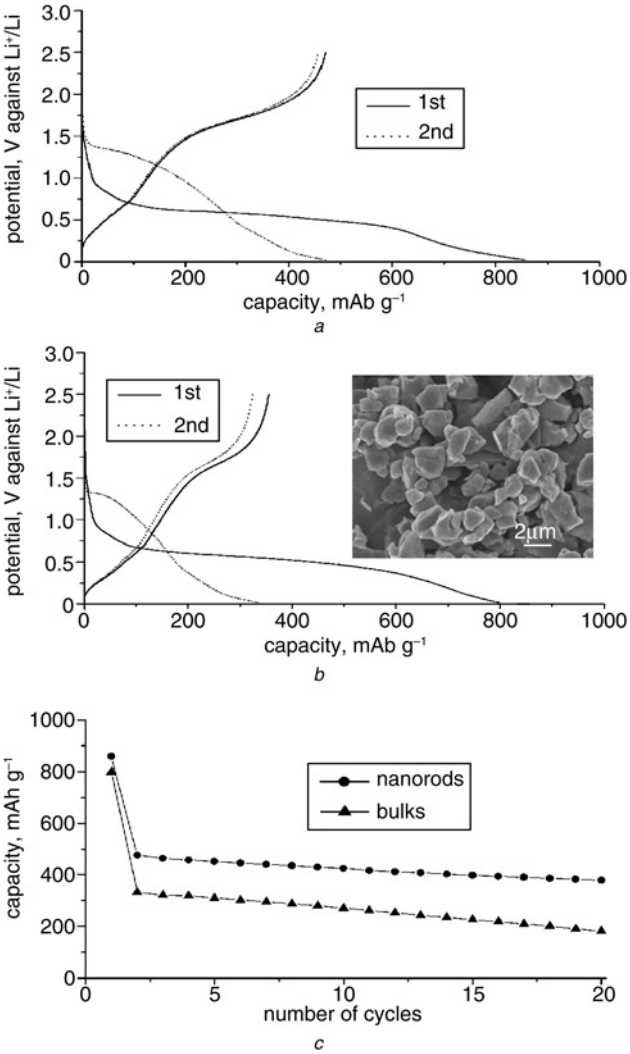

Figure 8 *Discharge/charge profiles of the Zn_2SiO_4*
a Nanorods
b Bulk materials for the first two cycles in the voltage range of 0.02–2.5 V
c Cycle stability of the Zn_2SiO_4 nanorods and bulk materials

the first cycle were 859 and 470 mAh g^{-1}, respectively. For the second discharge, the potential plateau shifted upwards to near 1.0 V (against Li^+/Li) with a more sloping profile accompanied by a capacity loss. The discharge and charge capacities decreased to 473 and 454 mAh g^{-1}, respectively. The irreversible capacity loss of the first cycle can be attributed to the formation of solid–electrolyte interphase film onto the surface of the electrode materials. For comparison purposes, we also evaluated the electrochemical performance of the Zn_2SiO_4 bulk materials obtained from the solid-state reaction (Fig. 8*b*). The inset of Fig. 8*b* displays the FESEM image of the bulk Zn_2SiO_4, from which it can be seen that the sample is composed of particles with typical sizes of about 2–4 μm. The initial discharge and charge capacities of the Zn_2SiO_4 bulk materials were 797 and 353 mAh g^{-1}, respectively. In the second cycle, the discharge and charge capacities reached 333 and 321 mAh g^{-1}. A comparison of the cycling performance between the Zn_2SiO_4 nanorods and the Zn_2SiO_4 bulk materials was carried out, which is shown in Fig. 8*c*. After 20 cycles, the retained reversible capacity of the Zn_2SiO_4 nanorods was 379 mAh g^{-1}, at a current density of 80 mA g^{-1}, whereas the Zn_2SiO_4 bulk materials retained only 181 mAh g^{-1}. Therefore, Zn_2SiO_4 nanorods show better discharge capacity and cyclability to Zn_2SiO_4 bulk particles. We believe the significantly improved electrochemical properties of the nanowire electrode may result from the following two effects. One is the relatively high specific surface areas of nanostructured materials, which provides more active sites for the contact between the active material and the electrolyte and decreases the polarisation of the electrode [5, 22]. The other factor is the fast kinetics related to the unique 1D nanostructured materials, which offer direct 1D electronic pathways, thus leading to efficient charge transport and faster electronic kinetics [22, 23].

4. Conclusion: In summary, Zn_2SiO_4 nanorods with high purity have been successfully fabricated using a facile template-free hydrothermal approach. The evolution of the composition and shape of the products were studied in detail and it was found that both reaction time and temperature play key roles in controlling the composition and shape of the Zn_2SiO_4 nanostructures. The Ostwald-ripening mechanism is proposed to explain the growth process of the Zn_2SiO_4 nanorods on the basis of the shape and phase evolution at continuous reaction time. Electrochemical measurements revealed that the Zn_2SiO_4 nanorods exhibited a higher discharge capacity and better cyclability than the Zn_2SiO_4 bulk materials. The reversible capacity of 379 mAh g^{-1} was delivered after 20 cycles at a current density of 80 mA g^{-1}.

5. Acknowledgments: The authors acknowledge support from the National Natural Science Foundation of China (no. 21303107), the Natural Science Foundation of Hebei Province (nos. B2014106056, B2010001946), and the Program of 'One Hundred Innovative Talents' of Higher Education Institutions of Hebei Province (no. BR2-264).

6 References

[1] Guo Y.P., Ohsato H., Kakimoto K.I.: 'Characterization and dielectric behavior of willemite and TiO_2-doped willemite ceramics at millimeter-wave frequency', *J. Eur. Ceram. Soc.*, 2006, **26**, pp. 1827–1830
[2] Bartohu C., Benoit J., Benalloul P., *ET AL.*: 'Mn^{2+} concentration effect on the optical properties of Zn_2SiO_4:Mn phosphors', *J. Electrochem. Soc.*, 1994, **141**, pp. 524–528
[3] Wang X.F., Huang H.T., Liu B., *ET AL.*: 'Shape evolution and applications in water purification: the case of CVD-grown Zn_2SiO_4 straw-bundles', *J. Mater. Chem.*, 2012, **22**, pp. 5330–5335
[4] Michalska I., Krysztafkiewicz A., Bogacki M.B., Jesionowski T.: 'Preparation and characterization of precipitated zinc silicates', *J. Chem. Technol. Biotechnol.*, 2003, **78**, pp. 452–460

[5] Zhang S.Y., Ren L., Peng S.J.: 'Zn_2SiO_4 urchin-like microspheres: controlled synthesis and application in lithium-ion batteries', *Cryst. Eng. Commun.*, 2014, **16**, pp. 6195–6202
[6] Yoon C., Kang S.: 'Synthesis of Zn_{2-x} Mn_x SiO_4 phosphors using a hydrothermal technique', *J. Mater. Res.*, 2001, **16**, pp. 1210–1216
[7] Wan J.X., Chen X.Y., Wang Z.H., *ET AL.*: 'One-dimensional rice-like Mn-doped Zn_2SiO_4: preparation, characterization, luminescent properties and its stability', *J. Cryst. Growth*, 2005, **280**, pp. 239–243
[8] An X.H., Meng G.W., Wei Q., *ET AL.*: 'Mesh-like hemispherical shells formed by self-assembly of Zn_2SiO_4 textured nanowires', *Cryst. Growth Des.*, 2006, **6**, pp. 1967–1971
[9] Yu X., Wang Y.H.: 'Synthesis and VUV spectral properties of nanoscaled Zn_2SiO_4:Mn^{2+} green phosphor', *J. Phys. Chem. Solids*, 2009, **70**, pp. 1146–1149
[10] Yang L.W., Wu X.L., Huang G.S., *ET AL.*: 'Self-catalytic synthesis and light-emitting property of highly aligned Mn-doped Zn_2SiO_4 nanorods', *Appl. Phys. A*, 2005, **81**, pp. 929–931
[11] Wang Y., Hao Y., Yuwen L.: 'Synthesis process dependent photoluminescent properties of Zn_2SiO_4:Mn^{2+} upon VUV region', *J. Alloy. Compd.*, 2006, **425**, pp. 339–342
[12] Morell A., Elkhiati N.: 'Green phosphors for large plasma TV screens', *J. Electrochem. Soc.*, 1993, **140**, pp. 2019–2022
[13] Li Q.H., Komarneni S., Roy R.: 'Control of morphology of Zn_2SiO_4 by hydrothermal preparation', *J. Mater. Sci.*, 1995, **30**, pp. 2358–2363
[14] Zhang Y.F., Fan M.J., Niu F., *ET AL.*: 'Hydrothermal synthesis of VO_2(A) nanobelts and their phase transition and optical switching properties', *Micro Nano Lett.*, 2011, **6**, (11), pp. 888–891
[15] Yu X., Wang Y.H.: 'Photoluminescent properties of nanoscaled Zn_2SiO_4:Mn^{2+} green phosphor under vacuum ultraviolet excitation', *J. Nanosci. Nanotechnol.*, 2010, **10**, pp. 1–4
[16] Wan J.X., Wang Z.H., Chen X.Y., *ET AL.*: 'Controlled synthesis and relationship between luminescent properties and shape/crystal structure of Zn_2SiO_4:Mn^{2+} phosphor', *J. Lumin.*, 2006, **121**, pp. 32–38
[17] Xu G.Q., Liu J.Q., Zheng Z.X., *ET AL.*: 'Low-temperature synthesis and luminescence properties of Zn_2SiO_4:Mn phosphors', *Chin. J. Lumin.*, 2011, **32**, pp. 550–554
[18] An J.S., Noh J.H., Cho I.S., *ET AL.*: 'Tailoring the morphology and structure of nanosized Zn_2SiO_4: Mn^{2+} phosphors using the hydrothermal method and their luminescence properties', *J. Phys. Chem. C*, 2010, **114**, pp. 10330–10335
[19] Stöber W., Fink A.: 'Controlled growth of monodi sperse silica spheres in the micron size range', *J. Colloid. Interf. Sci.*, 1968, **26**, pp. 62–69
[20] Li J., Zeng H.C.: 'Hollowing Sn-doped TiO_2 nanospheres via Ostwald ripening', *J. Am. Chem. Soc.*, 2007, **129**, pp. 15839–15847
[21] Peng Z.A., Peng X.G.: 'Mechanisms of the shape evolution of CdSe nanocrystals', *J. Am. Chem. Soc.*, 2001, **123**, pp. 1389–1395
[22] Zhang S.Y., Ci L.J., Liu H.R.: 'Synthesis, characterization, and electrochemical properties of $Cu_3V_2O_7(OH)_2{\cdot}2H_2O$ nanostructures', *J. Phys. Chem. C*, 2009, **113**, pp. 8624–8629
[23] Li W.Y., Cheng F.Y., Tao Z.L., *ET AL.*: 'Vapor-transportation preparation and reversible lithium intercalation/deintercalation of α-MoO_3 microrods', *J. Phys. Chem. B*, 2006, **110**, pp. 119–124

doi: 10.1049/mnl.2014.0250